EXPERIMENTALLY ISOLATING THE EFFECTS OF DENSITY AND POROSITY ON IMPACT CRATERS. C. J. Cline II[1] and M. J. Cintala[2]. [1]Jacobs, NASA Johnson Space Center, Houston, TX 77058 (christopher.j.cline@nasa.gov), [2]Astromaterials Research and Exploration Science Division, NASA Johnson Space Center, Code XI3, Houston, TX, 77058, USA.

Introduction: Relatively small impact craters offer a unique opportunity to glean insight into the near-surface properties of planetary bodies, as the morphometries and morphologies of these craters have been demonstrated to be influenced by the physical properties and structure of their targets [1-4]. With the latest generation of orbital cameras returning images of ever increasing resolution [5], populations of craters at the scales of a few meters are now being routinely analyzed [6-8]. Making the connection between crater morphometry and target properties on these poorly parameterized surfaces, however, requires carefully controlled laboratory experimentation to explore how changes in individual physical properties are expressed in the final crater. Here, we present the results of recent experiments that explore the effects of bulk target density and porosity on the cratering process.

Methodology: The six experiments presented here were conducted using the vertical gun housed in the Experimental Impact Laboratory at NASA Johnson Space Center. The targets were constructed using a variety of dry, cohesionless sands that filled cylindrical PVC buckets (26.2 cm diameter, 12.2 cm depth). Quartz, alumina (Al_2O_3), and garnet sands of similar grain-size distributions established a range of intrinsic densities of 2.56, 3.95, and 4.02 g cm^3, respectively. The target buckets were filled using two packing techniques: one in which the sand was quiescently poured into the buckets to create a relatively low-density/high-porosity target, and the other in which the sand was pluviated through a coarse-mesh sieve to create a relatively higher-density/lower-porosity medium. The combination of these materials and packing techniques yielded three targets (one of each material) that varied in bulk density but maintained a nearly constant porosity of 0.44.

Each target was impacted with a 4.76-mm aluminum sphere at 1.55±0.03 km s^{-1}, normal to the target's flat surface. Ejecta kinematics were determined by use of the Ejection-Velocity Measurement System (EVMS), originally detailed in [9]. This system uses a thin, vertically aligned laser sheet that can be strobed at a user-defined interval to illuminate the outer edge of the evolving ejecta curtain. A time-exposure of the event is recorded by a digital camera; such stroboscopic images permit the determination of radial ejection positions, ejection angles, and speeds of ejected particles.

Crater morphometry was determined by means of a high-resolution 3D scanner. Scans were collected immediately prior to and after the experiments. The point cloud data were then used to create topographic maps and cross sections of the craters (Fig.1 and 2).

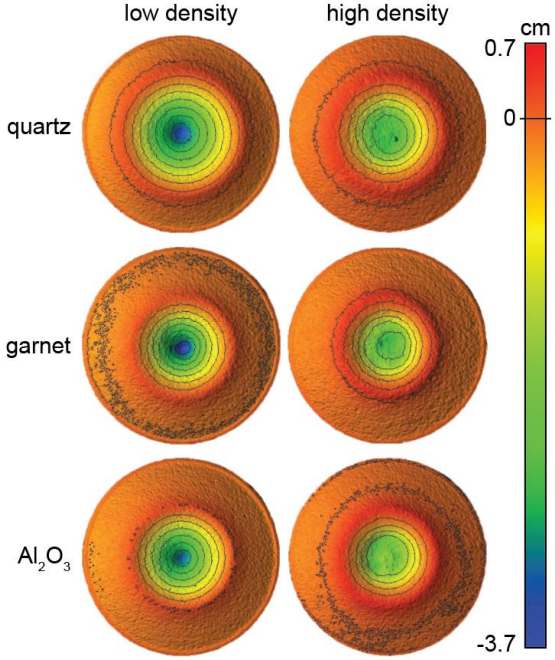

Figure 1. Topographic maps of the craters formed in the high- and low-density versions of each target material. The elevation scale is the same for all maps and is set such that 0 cm represents the pre-impact surface. Contour lines are in 0.5-cm increments from the lowest point in each crater.

Results: All craters, regardless of the target's packing technique or starting material, were morphologically simple (Fig. 1). Stark differences in morphometry, however, are immediately apparent between the targets of differing porosity. Craters formed in the more-porous targets exhibited conical cross sections, while those the less-porous ones were patently more bowl-shaped, had more voluminous rims, higher rims crests, smaller diameters, and were markedly shallower in all cases (Fig. 2).

The ejection speed of particles follows a power-law relationship with the scaled ejection position (Fig. 3). The fitting parameters fall within the bounds of energy and momentum scaling as described in [10, 11] and are similar to observations from other impact

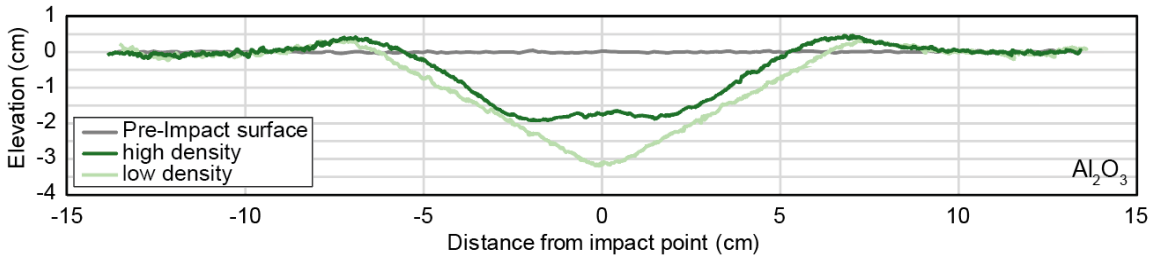

Figure 2. Crater profiles shown as at 1:1 scale. These profiles of the granular alumina targets are represetative of the general shape observed in the high- and low-density versions of the quartz and garnet targets.

experiments that used cohesionless sands [7, 10, and refs. therein]. The details of these fits, however, seem to be relatively insensitive to the differences in bulk target density and porosity. Ejection angles determined from all targets were steepest near the impact point (~50-53°) and decayed to a minimum near the crater rim (~40-45°). In general, the higher- porosity versions of each target are distinguished by marginally lower ejection speeds and higher ejection angles.

Discussion: The porosity of each target had a distinct effect on the morphometries of the final craters (Fig. 2). Lower-porosity targets exhibited depth-diameter ratios ~0.17, similar to those of the fresh lunar craters (<400 m in diameter) that were analyzed by [6], while the more-porous targets had ratios that ranged from 0.21 to 0.24, values that are more consistent with relatively large (>400 m diameter), fresh, simple lunar craters [6,12]. It is interesting to note that the craters formed in the less-porous targets also have flat floors, a morphology that has canonically been attributed to the presence of a subsurface cohesive horizon [1,6].

It is difficult to discern exactly what mechanism is responsible for the stark contrasts in crater shape within the limited scope of these experiments. Even though there appears to be a possible relationship between the depth-diameter ratio and porosity within the data set, this interpretation is complicated by consequential changes to other physical properties that were unable to be constrained as easily, such as the coefficient of static friction. We have attempted here to understand the ramifications of two isolated physical properties on the cratering process. It is clear, however, that much more work is ahead in probing the parameter space of relevant material properties, especially those that define the effective strength of a cohesionless target under the imposed stresses of an impact event.

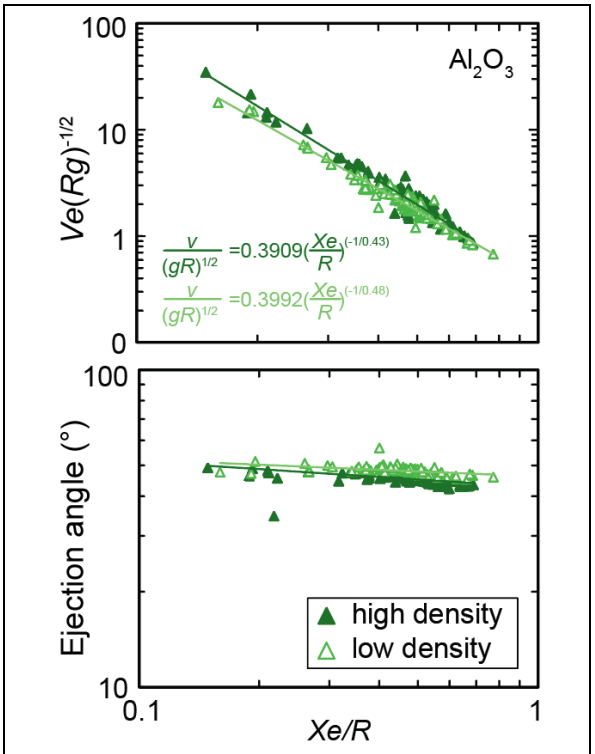

Figure 3. Ejecta kinematics for the alumina target determined from reconstructed ballistic trajectories. Scaled ejection speed and launch angle are plotted as a function of scaled ejection postion.

References: [1] Quaide and Oberbeck (1968) *JGR, 73*, 5247-5270. [2] Schmidt R. M. and Housen K. R. (1987) *Int. J. Impact engine., 5*, 543-560. [3] Wünnemann K. *et al.* (2011) *Proceed. XI Hypervel. Imp. Sym.* [4] Prieur A. C. *et al.* (2017) *JGR:Planets, 122*, 1704-1726. [5] Robinson M.S. et al. (2010) *SSR* 150:81-124. [6] Stopar J. D. *et al.* (2017) *Icarus, 298*, 34-48. [7] Walsh K.J. *et al.* (2019) *Nat. Geo* 12:242-246. [8] Noguchi R. *et al.* (2020) *Icarus* 354:114016. [9] Cintala M.J. *et al.* (1999) *Meteoritics and Planetary Sci.* 34, 605-623. [10] Housen K. R. *et al.* (1983) *JGR, 88, No. B3*, 2485-2499. [11] Housen K. R. and Holsapple K. A. (2011) *Icarus, 211*, 856-875. [12] Pike R. J. (1977) *LPSC VIII*, 3427-3436.